Topological Entropy and Homology Reveal Interpretable and Real-Time Neural Signatures in Pediatric EEG

Waleed Bin Owais, Herbert F. Jelinek, and Ibrahim (Abe) M. Elfadel

***Abstract*— Decoding neural states from pediatric EEG in naturalistic settings remains challenging due to signal noise, motion artifacts, and intersubject variability. This paper introduces *Enriched Topological Features* (ETF), a new approach integrating multiscale persistent homology ($\mathbb{H}_0$/$\mathbb{H}_1$), time-aggregated entropy via sliding windows, and Takens' phase-space embeddings to classify gameplay versus resting states in children. Using 4-channel EEG from 79 subjects recorded during museum-based *Minecraft* gameplay, ETF achieves 96.90% training accuracy and 94.96% test accuracy (F1 = 97.2%) with XGBoost classifiers, outperforming deep learning baselines by 21.3% and prior topological methods such as nonlinear EEG topological dynamics analysis (NETDA) by 3.0% in test accuracy. SHAP-based attribution reveals topological features reflecting distinct neural dynamics with gameplay engagement exhibiting elevated gamma-band persistence landscapes at frontal sites (AF8 $\mathbb{H}_1$ PL_2), indicating executive network recruitment, while resting states show high alpha-band entropy at temporal electrodes (TP9), reflecting metastable disengagement. The framework mitigates class imbalance through SMOTE and random undersampling, and captures developmental dynamics, including a significant negative correlation ($r = -0.23$, $p = 0.0176$) between frontal gamma topological stability and age, suggesting frontoparietal network maturation. With computational efficiency of 644 ms per epoch and consistent performance under noise, ETF offers interpretable, low-latency processing pipeline for pediatric mobile neurogaming and adaptive learning interfaces.**

***Index Terms*— Topological Data Analysis, Persistent Homology, Electroencephalography (EEG), Entropy, SHAP, XGBoost, SMOTE, Mobile Brain Imaging, Pediatric Neuroengineering**

I. Introduction

Understanding the neural basis of children's behavior in real-world settings remains a significant challenge in developmental neuroscience. Young children acquire cognitive, language, and social skills through dynamic, natural interactions, yet most neurophysiological studies still occur under solitary and highly controlled laboratory conditions [1]. Decoding pediatric electroencephalography (EEG) during naturalistic activities such as free play or gameplay with unconstrained movement offers more naturalistic cognitive insights into brain function that are directly relevant to children's everyday experiences [1].

The importance of studying the brain in ecologically valid contexts is widely recognized [2]. Observations in home or school environments tend to yield richer and more generalizable developmental findings than artificial tasks performed in laboratory settings [3]. In particular, early cognitive and social learning processes often arise through face-to-face interactions. Excluding natural social engagement from experimental paradigms may therefore limit both the validity and clinical relevance of developmental neuroscience research.

Moreover, advances in wearable EEG technology have made it possible to record brain activity outside of traditional lab environments [4]. This includes contexts where conventional participation is difficult such as children with autism who may find lab visits stressful, or families in remote communities. These developments reflect a growing effort to bridge the gap between lab based protocols and real-world pediatric neuroscience.

Conventional EEG paradigms, however, often fall short of this goal. Most developmental EEG studies restrict child movement and minimize environmental complexity typically instructing children to remain seated and view repetitive screen-based stimuli [5]. Adding to the challenge, children especially infants and toddlers are naturally active. Studies show that even during "calm" screen-based tasks, children move during the majority of recording time [6]. Such movement introduces artifacts that are difficult to suppress without either discarding large portions of data or removing meaningful neural signals [6]. These limitations highlight the need for alternative methods capable of tolerating motion while preserving signal interpretability.

To address these challenges, Mobile Brain-Body Imaging (MoBI) and mobile EEG systems have emerged as effective tools for studying brain activity during real-world behavior [7]. MoBI combines EEG with motion capture or inertial sensors, enabling participants to move freely while cognitive processes are recorded in context [8]. This approach treats movement not as noise but as meaningful cognitive data.

In this paper, EEG recorded from children engaged in naturalistic video game play is analyzed in a novel way to demonstrate that task related neural signatures can be

The first and third authors are with the Center of Secure Cyber Physical Systems and the Department of Computer and Information Engineering, Khalifa University, Abu Dhabi, UAE. The second author is with the Department of Medical Sciences & the Health Engineering Innovation Group, Khalifa University, Abu Dhabi, UAE. Corresponding author: Ibrahim (Abe) M. Elfadel (e-mail: ibrahim.elfadel@ku.ac.ae).

captured even under high-motion, real-world conditions. These findings underscore the feasibility of studying pediatric brain dynamics in situ and support the broader transition towards naturalistic developmental studies.

II. Related Work

Conventional EEG analysis techniques, such as band-power features, spectral decomposition, and functional connectivity, have been widely used for cognitive state classification. However, these methods often rely on assumptions of linearity and stationarity, which may not hold in real-world, non-stationary data settings [9]. This limitation becomes especially critical in pediatric EEG, where additional factors such as motion artifacts, high inter-subject variability, and short durations of artifact-free data further degrade signal quality and model robustness [10].

Deep learning approaches, including convolutional neural networks, have been used for automatic feature learning from EEG. Yet, their application in Mobile Brain Body Imaging (MoBI) contexts is constrained by practical limitations such as low density EEG systems, small and noisy datasets, and inconsistent recording conditions [11]. Prior studies using neural networks to differentiate rest from task states under similar constraints have reported only modest classification performance, highlighting the difficulty of extracting generalizable neural features in mobile, pediatric settings. [11]

Furthermore, traditional signal processing and machine learning methods often reduce brain dynamics to pairwise associations, which limits their ability to capture the complex, high order interactions inherent in neural activity [12]. To address this, nonlinear time series analysis techniques such as entropy measures, fractal dimensions, and phase space reconstruction have been introduced. While these methods provide deeper insights into EEG complexity, they often suffer from limited flexibility across subjects, time frames, and recording conditions.

Recent advances in topological signal processing (TSP) have provided noise-tolerant methods [10]. By applying persistent homology to phase space embeddings of EEG signals, TSP captures the geometric structure of neural dynamics in a manner that is resilient to noise and sampling variability. This topological perspective has shown utility in tasks such as neurodegenerative disease classification and offers potential for decoding cognitive states in complex scenarios like gameplay [13].

A notable application of this approach is the nonlinear EEG topological dynamics analysis (NETDA) framework [14], which applied topological data analysis to pediatric EEG recorded during gameplay in a real world setting. NETDA achieved high classification accuracy in distinguishing rest from gameplay states by extracting persistence landscapes from phase space representations [14]. Its strength lies in exploiting the noise tolerance of topological data analysis (TDA) and its suitability for low-channel EEG, making it viable for mobile neuroimaging. However, the framework also presents key limitations, including sensitivity to embedding parameters, lack of interpretability for topological features, and the absence of class imbalance correction. While NETDA represents a meaningful step in adapting TDA to naturalistic pediatric EEG, further work is needed to benchmark it against deep learning models and to assess its scalability across datasets and populations.

This work introduces the first interpretable topological framework for pediatric EEG classification in naturalistic settings, combining persistence landscapes with entropy based features across multiple homology dimensions. Building on the foundation laid by NETDA, this approach enhances efficacy through artifact-validated epoch filtering, class imbalance correction, and cost-sensitive learning challenges largely overlooked in prior work. Unlike deep learning pipelines that demand complex architectures and offer limited interpretability, this method is modular and computationally efficient, and optimized for real-time inference. This study improves on prior work in classification accuracy and interpretability for decoding cognitive brain states from low-density mobile EEG in pediatric populations.

III. Topological Foundations of Feature Extraction

A. Vietoris–Rips Complexes and Simplicial Filtration

Topological Data Analysis (TDA) offers a formalism for capturing the intrinsic structure of data through topological invariants. Central to this framework is the notion of a *simplicial complex*, a combinatorial structure that generalizes graphs to higher dimensions. A k-simplex consists of $k+1$ affinely independent points; examples include 0-simplices (vertices), 1-simplices (edges), 2-simplices (triangles), and so on [15].

For a finite point cloud $X \subset \mathbb{R}^d$, the Vietoris–Rips complex $\mathcal{R}(X,\epsilon)$ at scale $\epsilon > 0$ is defined as the set of simplices $\sigma \subset X$ for which all pairwise distances between points in σ are at most ϵ:

$$\mathcal{R}(X,\epsilon) = \{\sigma \subset X \mid \mathrm{diam}(\sigma) \leq \epsilon\}. \tag{1}$$

As ϵ varies, these complexes form a filtration that encodes the data's shape across multiple spatial resolutions.

B. Persistent Homology and Multiscale Topology

The evolution of topological features across a filtration is quantified using persistent homology. Each topological structure such as a connected component or loop is tracked by its birth and death scales, forming a homology class H_k, where $k = 0$ corresponds to connected components and $k = 1$ denotes one-dimensional cycles [16].

Each feature is represented as a birth–death pair (b_i^k, d_i^k), with persistence (or lifetime) defined as:

$$\ell_i^k = d_i^k - b_i^k. \tag{2}$$

The set of all such pairs forms a persistence diagram, which summarizes topological lifespans. Barcode plots are

commonly used to visualize this information, with blue lines denoting H_0 features and red lines representing H_1 features.

C. Topological Descriptors: Landscapes and Entropy

While persistence diagrams are extensive in information, they are not directly amenable to vector-based analysis. To overcome this, persistence landscapes transform diagrams into functions in a Hilbert space, enabling consistent and differentiable representations [17]. These are constructed by projecting birth–death intervals onto piecewise-linear functions, retaining the most significant layers for further analysis.

In addition, persistence entropy [18] serves as a compact summary of diagram complexity. For a persitence diagram $D = \{(b_i, d_i)\}$, the persistence entropy is given by:

$$\mathrm{PE}(D) = -\sum_i p_i \log p_i, \tag{3}$$

$$p_i = \frac{d_i - b_i}{\sum_j (d_j - b_j)}. \tag{4}$$

This measure reflects the spread and uniformity of topological lifespans within a given homology dimension and provides a scalar descriptor of structural regularity.

IV. Dataset Description

This study utilized the publicly available Mobile Brain-Body Imaging (MoBI) dataset, collected at the Children's Museum of Houston [19]. It comprises electroencephalogram (EEG) and accelerometer recordings from 232 children (ages 6–16; mean age: 8.7 ± 2.2 years) engaged in naturalistic, museum-based gameplay. Each participant completed a 1-minute eyes-open resting baseline followed by up to 20 minutes of Minecraft gameplay in a real-world environment.

EEG signals were recorded using a 4-channel Muse headband (TP9, TP10, AF7, AF8) at a sampling rate of 220 Hz, with an online 60 Hz notch filter. Concurrently, 3-axis head motion was captured via onboard accelerometers at 50 Hz. The dataset includes raw EEG, head movement signals, and annotated time markers for task segmentation.

After preprocessing and quality control, a total of **79 subjects** were retained for downstream analysis. Subjects were excluded if any required segmentation markers (`baseline_start`, `baseline_end`, `task_start`, `task_end`) were missing, or if the data did not yield a sufficient number of valid 4.5-second epochs for both rest and gameplay conditions.

From this final cohort, 345 rest and 5771 gameplay epochs were extracted, resulting in a severe class imbalance of approximately 16:1. This skew arises not from sampling bias but from the experimental design itself, where only one minute of resting-state EEG was recorded versus an extended gameplay session. Rather than discarding informative gameplay data, we retained the full context and employed targeted balancing techniques including random undersampling, Synthetic Minority Oversampling Technique (SMOTE), and cost-sensitive learning to ensure statistically fair and representative evaluation, especially for the underrepresented rest condition.

Algorithm 1 *Feature extraction and classification with Enriched Topological Features (ETF)*

Require: EEG tensor $\mathcal{X} \in \mathbb{R}^{N \times M \times T}$, embedding parameters ($m = 4$, $\tau = 5$), window size w, step size s, frequency bands $\mathcal{B} = \{\theta, \alpha, \beta, \gamma\}$, maximum homology $k = 1$
Ensure: Feature matrix $\mathbf{U}$, labels $\mathbf{y}$, subject groups $\mathcal{G}$

```
for each subject i = 1 to N do
    Extract rest and gameplay intervals using annotated markers
    Apply preprocessing filters to each EEG channel:
    • High-pass filter at 1 Hz to remove DC offset and low-frequency drift
    • Notch filter at 60 Hz to remove line noise
    • Low-pass filter at 35 Hz to constrain signal within EEG band
    for each EEG channel j = 1 to M do
        for each band b ∈ {θ : 4 − 8 Hz, α : 8 − 13, β : 13 − 30, γ : 30 − 35}
        do
            Apply FIR bandpass filter to extract x_{b,j} for band b
            for each time window w of T in x_{b,j} (size w, step s) do
                Takens embedding Φ(w) = [x_t, x_{t+τ}, x_{t+2τ}, x_{t+3τ}]
                Compute persistence diagrams H_0, H_1 via Vietoris–Rips
                Compute landscapes λ^b_{0,j}, λ^b_{1,j} (resampled to d = 30)
                Compute entropies for each homology:
                    E^b_{0,j} = −Σ_i p_i log p_i,   p_i = ℓ_i / Σ_j ℓ_j,   ℓ_i = d_i − b_i
                (Repeat for E^b_{1,j})
            end for
        end for
    end for
    for each time window w of T do
        Concatenate all features across bands and channels for each subject j
        on a per-window basis:
            u_j(w) = [λ^b_{0,j}, λ^b_{1,j}, E^b_{0,j}, E^b_{1,j}]_{∀b∈B,j}
        Temporal aggregation: u_j^(w) = mean[u_j(w)]
    end for
end for
Class Balancing:
Option 1: Apply SMOTE (minority → 50–70%) to training folds only
Option 2: Random undersampling of gameplay epochs per subject
Classifier Evaluation:
for each classifier f ∈ {RF, XGB, SVM, DT} do
    Assign class weights: {0 : 18.0, 1 : 1.0}
    Perform 5-fold GroupKFold (subject-wise)
    Train on D_train, test on D_test
    Record training/test accuracy, class-wise precision, recall, F1-score
end for
```

The raw EEG and accelerometer data used in this study were obtained directly from the publicly released `.mat` files provided by the authors of the data sets. No proprietary Muse preprocessing tools (e.g., Muse SDK, MuseDirect) were used. All data cleaning, epoch segmentation, and artifact removal were performed using a custom MATLAB pipeline, as described in Section V.

Importantly, ecologically valid pediatric EEG datasets that are collected from freely-behaving children in dynamic, non-clinical settings remain exceedingly rare. The MoBI dataset uniquely enables the study of brain dynamics during naturalistic gameplay, supporting the development of noise-resilient, generalizable models for pediatric brain-computer interface applications.

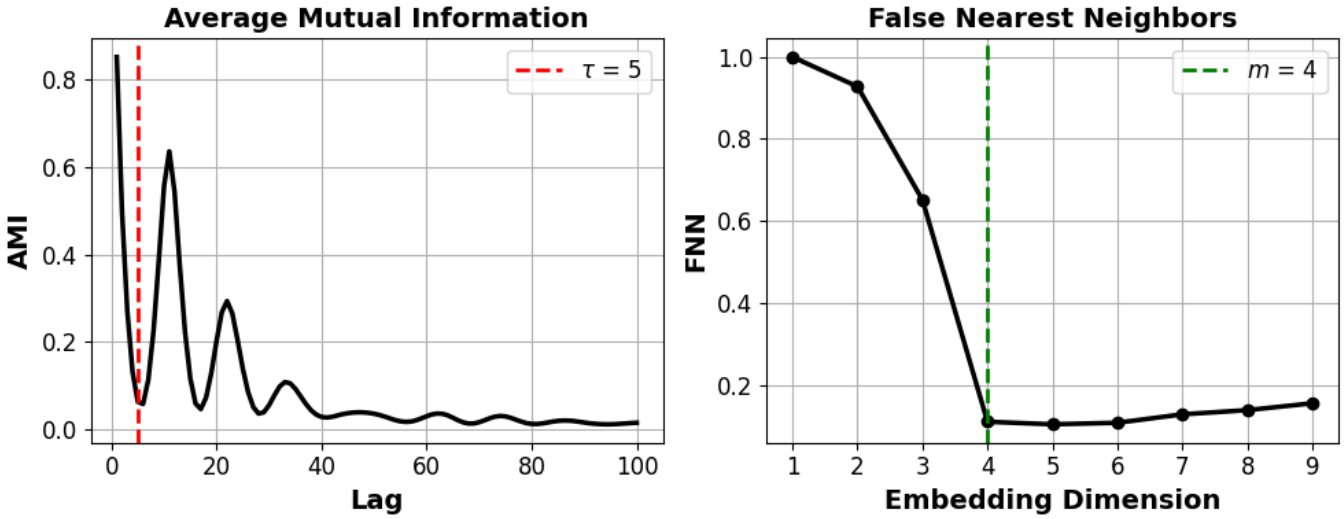

Fig. 1: Estimation of phase-space embedding parameters via Average Mutual Information (AMI) and False Nearest Neighbors (FNN) analysis for Subject 29. (Left) The AMI curve quantifies mutual information between the EEG signal and its time-delayed copies as a function of lag. The first local minimum occurs at $\tau = 5$, indicating the optimal delay that decorrelates the signal while preserving underlying structure. (Right) The FNN curve shows the proportion of false nearest neighbors as a function of embedding dimension m. The curve sharply drops at $m = 4$, suggesting sufficient unfolding of the attractor in phase space. Together, these results justify the use of fixed parameters $\tau = 5$ and $m = 4$ across all recordings, as they align with the most frequently observed optimal values across subjects.

V. Feature Extraction and Classification with Enriched Topological Features (ETF)

The Enriched Topological Features (ETF) framework is designed to decode cognitive brain states from low-density pediatric EEG recorded in naturalistic environments. It combines topological signal processing with entropy-based temporal summarization to capture nonlinear patterns in brain activity while remaining stable under real-world noise and variability. To handle class imbalance and subject heterogeneity, ETF uses both random undersampling and synthetic oversampling methods. The pipeline is modular, interpretable, and computationally efficient, making it suitable for mobile neuroimaging and time-sensitive applications. The method is summarised in Algorithm 1.

A. Preprocessing and Signal Transformation

EEG data were acquired from four Muse headband channels (TP9, TP10, AF7, AF8) at a sampling rate of 220 Hz. Recordings were segmented into rest and gameplay intervals using manually validated event markers embedded in the recording metadata. To enhance signal fidelity and suppress non-neural artifacts, a structured preprocessing pipeline was applied. First, the raw signals were high-pass filtered at 1 Hz using a zero-phase 4th-order Butterworth filter to remove DC offset and low-frequency drift. Next, a notch filter centered at 60 Hz was applied to attenuate line noise contamination [20], followed by a low-pass filter at 45 Hz to constrain the signal within the canonical EEG band. The resulting band-limited signals were then divided into non-overlapping 4.5-second epochs.

Each epoch was assessed for signal quality using multiple criteria. Epochs exhibiting excessive amplitude fluctuations defined as a standard deviation exceeding 75 μV on any channel were marked as noisy and excluded. Conversely, epochs with abnormally low variance (standard deviation below 0.05 μV) were flagged as flatlined, often indicating sensor detachment or hardware malfunction. To address potential electromyographic (EMG) interference, power spectral density (PSD) was estimated using Welch's method [21], and epochs where the gamma band (35–45 Hz) accounted for more than 25% of total power on any channel were discarded. Additionally, line noise contamination was evaluated by comparing spectral power in the 48–52 Hz band to surrounding frequencies (40–60 Hz); epochs with line noise power exceeding twice the local baseline were excluded. Only epochs that passed all artifact checks across all channels were retained for subsequent analysis, ensuring high-quality, artifact-free EEG data.

Each band-limited EEG signal was transformed via phase-space reconstruction (PSR) using Takens' embedding theorem [22] to recover the underlying state-space dynamics. To determine suitable embedding parameters, Average Mutual Information (AMI) [23] and False Nearest Neighbors (FNN) [24] analyses were conducted across the full subject cohort. AMI was used to estimate the time delay (τ) by locating the first local minimum in the mutual information curve, while FNN identified the embedding dimension (m) by determining the point at which the proportion of false neighbors dropped below 10%. These analyses yielded highly consistent results, with τ values concentrated around 5 and m values most frequently be-

tween 3 and 4. Based on these trends, fixed values of $\tau = 5$ and $m = 4$ were adopted for all recordings, as they closely matched the parameters selected based on cohort-level trends in AMI and FNN. for the majority of subjects while also supporting consistency and computational efficiency. This yielded embedded trajectories of the form:

$$\Phi(x_t) = [x_t, x_{t+\tau}, x_{t+2\tau}, x_{t+3\tau}] \in \mathbb{R}^4, \tag{5}$$

which preserves the geometric structure of temporal evolution and serves as input to the topological analysis pipeline described in the following section. Representative AMI and FNN curves of one subject are shown in Figure 1 to illustrate the typical trends observed across the dataset.

B. Topological Feature Extraction

Topological data analysis (TDA) was used to capture structural properties of EEG signals. For each phase-space-reconstructed (PSR) trajectory, persistent homology was computed up to dimension 1 using Vietoris–Rips complexes. Two topological descriptors were derived from the resulting persistence diagrams:

- **Persistence Landscapes (PL):** Birth–death intervals of $\mathbb{H}_0$ and $\mathbb{H}_1$ (connected components and loops, respectively) were transformed into one-dimensional persistence landscapes. Each landscape was sampled at 30 uniformly spaced evaluation points, producing fixed-length feature vectors.
- **Persistence Entropy (PE):** Each persistence diagram D was also summarized by its entropy:

$$E(D) = -\sum_i p_i \log p_i, \quad p_i = \frac{\ell_i}{\sum_j \ell_j}, \quad \ell_i = d_i - b_i \tag{6}$$

  where (b_i, d_i) denote the birth and death times of the i-th topological feature.

Each EEG epoch was ultimately represented as a fixed-length feature vector, composed of persistence landscapes (30 values) and persistence entropy (1 value) computed across four frequency bands (theta, alpha, beta, gamma), two homology dimensions ($\mathbb{H}_0$, $\mathbb{H}_1$), and either two channels (TP9, TP10) or all four Muse channels (TP9, TP10, AF7, AF8). This resulted in feature vectors of 496 dimensions for the 2-channel configuration and 992 dimensions for the 4-channel configuration. These descriptors were extracted for each sliding window and averaged over time to yield a single vector per epoch. This high-resolution representation captures both the geometric structure and complexity of neural activity across multiple spatiotemporal scales.

To capture nonstationary signal behavior, a sliding-window approach was applied within each EEG epoch using a window length of 330 samples and a step size of 110 samples. Features were extracted per window and averaged across all windows, resulting in a single time-aggregated feature vector per epoch. Figure 2 illustrates representative topological signatures derived from Subject 27's EEG data, highlighting differences in barcodes, persistence diagrams, and landscapes between gameplay and rest states.

C. Class Balancing and Feature Integration

To mitigate the severe class imbalance between rest and gameplay epochs, two class balancing strategies were implemented during training: oversampling with SMOTE [25] and cost-sensitive learning, and within-subject random undersampling [26].

In the *oversampling configuration*, SMOTE was applied within each training fold to synthetically generate minority class (rest) samples by interpolating between neighbors in the feature space. This increased the representation of the minority class to 50–70% of the majority class size, depending on the fold. To further enhance sensitivity to rest epochs, *class weighting* was introduced during classifier training, assigning 18–25× higher misclassification penalties to rest epochs than gameplay epochs. This penalization discouraged trivial majority-class predictions and encouraged the model to better detect underrepresented rest states. In the *undersampling configuration*, a random subset of gameplay epochs was selected without replacement to match the number of rest epochs within each subject. This approach preserved within-subject balance and data authenticity, albeit at the expense of gameplay sample diversity. To evaluate the plausibility of SMOTE-generated samples, we conducted principal component analysis (PCA) on the resampled ETF feature space. The first two principal components captured 75.79% of the total variance, allowing visualization of the geometric structure of synthetic and real data in a reduced space. As shown in Figure 3, synthetic rest samples (blue) overlapped with gameplay samples (red) within a shared manifold, suggesting that interpolation in topological feature space preserved statistical coherence. Notably, synthetic points did not form outlier clusters or deviate from the native distribution, supporting the validity of SMOTE in high-dimensional persistence landscape and entropy representations.

In both setups, each EEG epoch was represented by a unified feature vector composed of persistence landscapes and entropy values derived from $\mathbb{H}_0$ and $\mathbb{H}_1$ diagrams across four canonical EEG bands and selected posterior-temporal channels (TP9, TP10). The final feature representation is defined as:

$$\mathbf{u} = [\lambda_0, \lambda_1, E_0, E_1] \in \mathbb{R}^d, \tag{7}$$

where $\lambda_k, k = 0, 1$, is a vector of persistence landscape functions sampled and $E_k, k = 0, 1$, denotes the persistence entropy. Recall that $k = 0, 1$ denotes the homology dimension for connected components ($k = 0$) and 2D cycles ($k = 1$).

D. Classification and Evaluation

Four supervised classifiers were selected to benchmark the proposed topological features across a spectrum of model complexities and interpretability. XGBoost (XGB) was chosen due to its strong performance in imbalanced, high-dimensional data settings and proven utility in EEG classification [27]. Random Forest (RF) offers resilience to noise and feature redundancy, making it ideal for topological EEG features [14]. Support Vector Machine (SVM) with

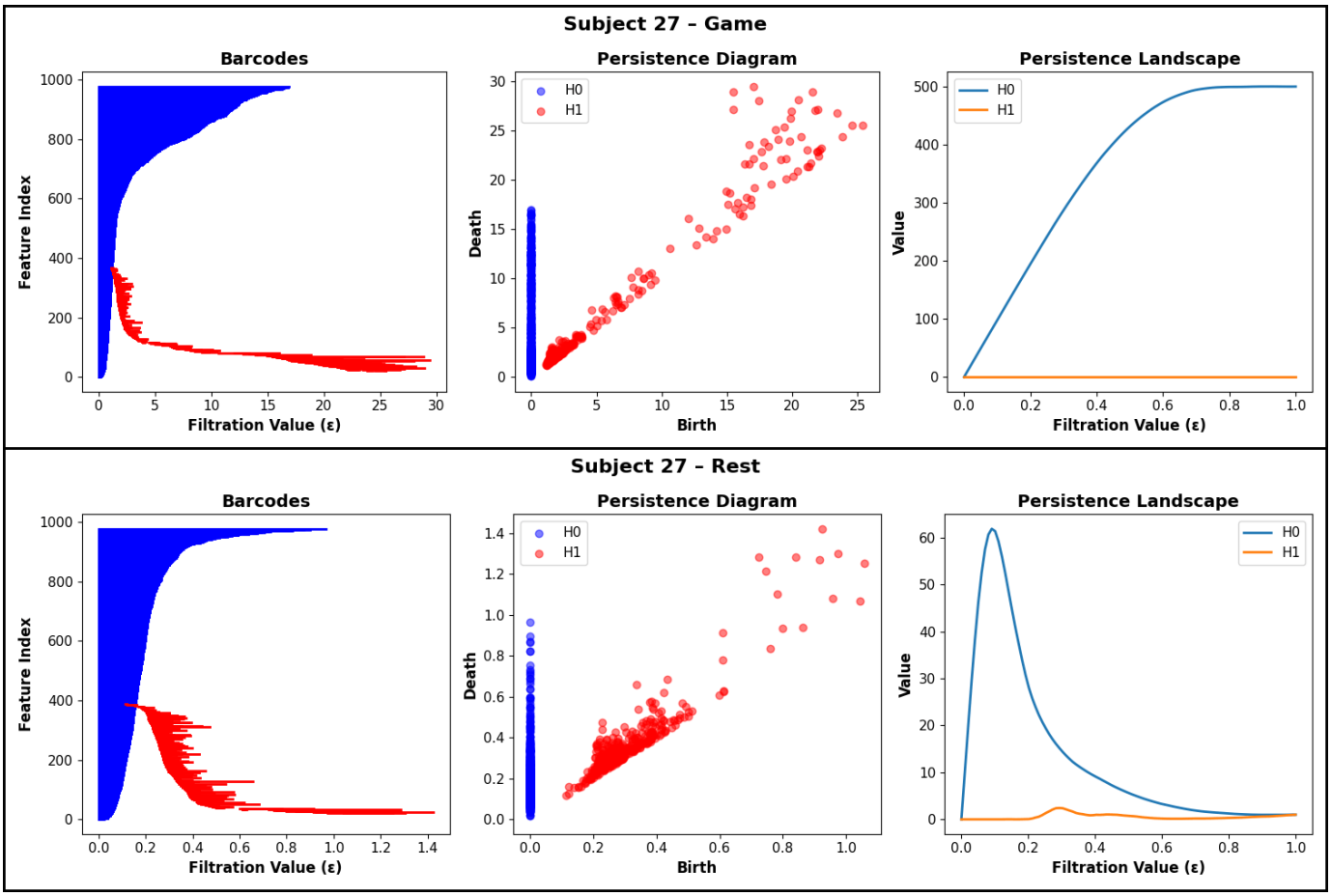

Fig. 2: Topological data analysis (TDA) of EEG signals from Subject 27 (channel AF8, Gamma band). The top row shows the barcode, persistence diagram, and persistence landscape for the **gameplay** state; the bottom row shows the same features for the **rest** state. The x-axis in the barcode and landscape plots denotes the filtration value (ϵ), and the persistence diagram visualizes birth-death pairs of topological features in $\mathbb{H}_0$ (blue) and $\mathbb{H}_1$ (red).

RBF kernel enables nonlinear decision boundaries, while Decision Tree (DT) provides an interpretable baseline with clear rule-based structure [28], [29].

To assess classification performance, 5-fold cross-validation was conducted using the GroupKFold strategy [30], which ensures subject-level independence by assigning all EEG segments from a given participant to the same fold. For each fold, class balancing was applied exclusively to the training split using one of two strategies: (i) SMOTE, or (ii) random undersampling of the majority class (gameplay epochs). The test set was left unmodified to retain the original class proportions in test data and enable realistic performance evaluation.

Class weights were explicitly specified in each classifier to penalize misclassification of the minority class. Each EEG segment was represented by a feature vector of 496 or 992 dimensions depending on whether 2 or 4 EEG channels were used, respectively.

Model performance was quantified using standard classification metrics: accuracy, precision, recall, and F1 score, computed independently for each class and reported separately for training and testing subsets. Mean scores were calculated across the five cross-validation folds to ensure reliable performance estimates [31].

All experiments were repeated under two spatial configurations:

1) A reduced 2-channel setting using TP9 and TP10 (temporal electrodes), and
2) A full 4-channel setting using all Muse electrodes (TP9, TP10, AF7, AF8).

All feature extraction and classification procedures were implemented in Python 3.12 using standard scientific computing libraries, including NumPy, SciPy, scikit-learn, and matplotlib. Topological features were computed using `ripser.py` and `giotto-tda`, while data balancing was handled using `imblearn`. All computations were executed on a machine with an Intel Core i7-11800H CPU (8 cores, 2.30 GHz) and 32 GB DDR4 RAM.

VI. Results

Table I presents a comprehensive comparison of classification performance across previously published methods, the NETDA pipeline, and the proposed Enriched Topological Feature (ETF) framework, evaluated under both SMOTE and random undersampling regimes. Results are

TABLE I: Comparison of classification performance with prior work and the proposed Enriched Topological Feature (ETF) approach using pediatric EEG data. “TP9, TP10” refers to models trained using only the two temporal electrodes available on the Muse headset, while “All 4” indicates the inclusion of all available Muse channels (TP9, TP10, AF7, AF8). ETF features include persistence landscapes and entropy measures extracted from both $\mathbb{H}_0$ and $\mathbb{H}_1$ topological dimensions across theta, alpha, beta, and gamma frequency bands. Classifier performance is reported as the mean across 5-fold GroupKFold cross-validation, with a subject-independent split ratio of 80:20 (train:test). Per-class metrics are shown only for class 1 (game). The hyphen “–” indicates the metric was not reported or not statistically tested.

Method	**Channels**	**Classifier**	**Train Acc (%)**	**Test Acc (%)**	**Prec (%)**	**Rec (%)**	**F1 (%)**	***p*-val**
DL [11]	TP9, TP10	–	–	67.4	67.99	65.55	66.80	–
	All 4	–	–	73.68	72.91	71.40	72.15	–
NETDA [14]	TP9, TP10	RF	–	89.71	90.90	88.46	89.71	–
		SVM	–	87.96	91.50	86.71	87.96	–
		DT	–	83.08	84.27	81.33	83.08	–
	All 4	RF	–	91.96	92.72	91.21	91.96	–
		SVM	–	89.92	90.68	89.17	89.92	–
		DT	–	88.22	88.98	87.47	88.22	–
ETF (SMOTE) - This work	TP9, TP10	RF	91.94	89.58	95.3	93.0	94.1	–
		XGB	95.51	94.78	96.2	94.8	95.5	1.65e−07
		SVM	72.69	63.67	90.7	59.0	72.0	–
		DT	93.68	94.90	89.0	87.5	88.2	–
	All 4	RF	95.20	92.28	97.3	95.7	96.4	–
		XGB	96.90	94.96	98.2	96.3	97.2	2.79e−04
		SVM	78.85	69.88	93.9	67.2	78.2	–
		DT	94.63	94.90	97.1	95.9	96.5	–
ETF (Undersample) - This work	TP9, TP10	RF	91.13	68.85	97.0	69.0	81.0	–
		XGB	95.94	68.56	98.0	68.0	80.0	0.313
		SVM	54.57	32.96	95.0	20.0	32.0	–
		DT	84.79	65.45	97.0	66.0	79.0	–
	All 4	RF	95.21	73.62	96.0	74.0	83.0	–
		XGB	99.06	71.15	96.0	73.0	83.0	0.300
		SVM	54.28	57.15	92.0	57.0	71.0	–
		DT	86.31	67.27	95.0	70.0	81.0	–

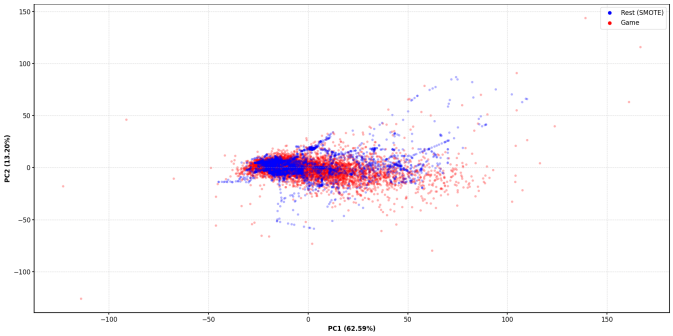

Fig. 3: Principal Component Analysis (PCA) of ETF features after SMOTE oversampling. The first two principal components (PC1 and PC2) account for 75.79% of the variance. Blue points denote synthetic "rest" epochs generated by SMOTE, while red points represent real "gameplay" epochs. The overlap between both classes in the projected space suggests that SMOTE interpolation preserves the statistical structure of topological EEG features.

reported for both the two-channel (TP9, TP10) and full four-channel (TP9, TP10, AF7, AF8) Muse EEG configurations, using Random Forest (RF), XGBoost (XGB), Support Vector Machine (SVM), and Decision Tree (DT) classifiers. All models were trained and evaluated using 5-fold subject-wise GroupKFold cross-validation with an 80:20 train-test split. For each configuration, class-wise precision, recall, and F1-score are shown alongside training and test accuracies. Paired *t*-tests with Bonferroni correction were conducted to assess the statistical significance of XGBoost's performance over other classifiers.

Under the SMOTE condition, ETF consistently outperformed both NETDA and prior deep learning baselines across nearly all metrics. With all four EEG channels, XGBoost achieved the highest test accuracy of 94.96%, with a training accuracy of 96.90%. It also yielded the best F1 score (97.2%) for the majority class (game) and maintained moderate performance on the minority class (rest), with class-wise precision and recall of 26.0% and 36.0%, respectively. RF and DT also demonstrated strong performance under SMOTE, achieving test accuracies above 92%, and F1 scores for class 1 above 96%. In the reduced TP9, TP10 configuration, XGBoost maintained excellent generalization with a test accuracy of 94.78% and balanced F1 scores (35.0% for rest, 95.5% for game). Statistical analysis confirmed that XGBoost significantly outperformed SVM and DT across both channel setups under SMOTE ($p < 0.01$), while its advantage over RF was not statistically significant but showed a consistent trend.

In contrast, the ETF framework under random undersampling exhibited a clear degradation in test performance. This reduction is largely attributable to the loss of informative training samples from the majority class during balancing. Even though XGBoost again produced

the highest training accuracy (99.06%), its test accuracy dropped to 71.15% with all four channels and further declined to 68.56% in the TP9, TP10 setting. Class-wise F1 scores for the minority class (rest) remained low (35.0% and 21.0%, respectively), indicating reduced sensitivity to class imbalance. SVM and DT classifiers, in particular, showed considerable instability under undersampling, with SVM test accuracies falling below 58% across both channel sets. The p-values for XGBoost comparisons under undersampling were non-significant ($p = 0.300$–0.313), further highlighting the limitations of this strategy in preserving classifier efficacy.

SMOTE improved test performance more consistently than undersampling. While undersampling truncates the dataset to balance class proportions often at the cost of discarding valuable information SMOTE synthetically augments the minority class without altering the majority distribution. This allows the classifier to generalize more effectively, especially in high-dimensional feature spaces like those derived from topological descriptors. In the context of pediatric EEG data, where minority-class (rest state) samples are inherently sparse, preserving minority class variability is important for detecting low-salience neural patterns.

VII. Feature Analysis

SHAP analysis [32] was conducted using TreeExplainer on an XGBoost classifier trained with features extracted via the ETF pipeline. Each EEG epoch was bandpass filtered, embedded using Takens delay coordinates and transformed into persistence diagrams via Vietoris–Rips filtration. From these, persistence landscapes and entropy values were computed for $\mathbb{H}_0$ and $\mathbb{H}_1$ across all frequency bands and EEG channels. Features were averaged across sliding windows to yield a fixed-size vector per epoch. SHAP values were computed on the resulting feature matrix, and mean absolute SHAP values were used to rank feature importance. Feature names were mapped to their corresponding frequency band, channel, homology dimension, and type (landscape or entropy) for interpretability.

A. Key Topological Features

Figures 4(a) and 4(b) display the most impactful features as identified by SHAP analysis. Gamma-band persistence landscapes (PL) in frontal electrodes and entropy-based features in the alpha band emerged as dominant contributors:

- **Gamma (AF8) $\mathbb{H}_1$ PL 2** produced the highest mean |SHAP| value (0.16), indicating strong predictive influence during gameplay epochs. This finding is consistent with prior associations between gamma activity and task-relevant attention, sensorimotor coordination, and frontal executive engagement.
- **Alpha (TP9) $\mathbb{H}_1$ PL 15 and 19**, along with **Gamma (TP9) $\mathbb{H}_1$ PL 6**, yielded large negative SHAP values (mean: −0.4 to −0.6), signifying a stronger association with rest-state neural dynamics characterized by sustained alpha topological structure.
- **Entropy features** (e.g., Gamma $\mathbb{H}_1$ entropy at AF8) showed mixed directionality, reflecting shifts in neural complexity across behavioral states. Such bidirectional influence suggests state-dependent modulation of cortical variability.

B. Neurocognitive Interpretation

The dominance of frontal gamma PL (notably at AF8) aligns with increased cognitive load and prefrontal network activation during gameplay. Gamma oscillations are linked to fast cortical computations and working memory maintenance processes heavily recruited during complex visuospatial tasks such as *Minecraft* [33] [34].

In contrast, posterior alpha PL components, especially at TP9, were indicative of resting-state conditions, consistent with alpha's role in sensory inhibition and default-mode network stability. These features suggest preservation of alpha-dominant dynamics during cognitive disengagement [35].

Beta-band asymmetries were also observed. For example, **Beta (AF7) $\mathbb{H}_1$** PL 10 showed stronger positive SHAP contributions toward gameplay prediction, while right-posterior counterparts (e.g., **TP10**) displayed reduced influence. This lateralization is suggestive of left-hemisphere dominance in visuomotor coordination, consistent with functional beta–gamma coupling observed during top-down motor control [36].

C. Topological Signatures of Cognitive Load

Entropy and persistence landscape features revealed interpretable markers of task-induced neural reconfiguration. Reduced alpha-band entropy during gameplay suggests a suppression of spontaneous cortical fluctuations, potentially reflecting constrained neural flexibility under elevated executive demand [37]. Concurrently, elevated gamma-band persistence landscape complexity particularly at frontal site AF8 indicates a reorganization of local neural assemblies, consistent with increased functional integration within frontal circuits during cognitively demanding tasks [33].

D. Clinical and Developmental Relevance

The observed gamma-alpha decoupling and hemispheric asymmetries hold particular relevance for pediatric neurodevelopment [38]. Frontal gamma amplification could reflect compensatory mechanisms in developing cortico-cortical networks during tasks demanding top-down control. Additionally, beta-band lateralization implicates parietal-premotor pathways in early-stage motor learning, highlighting the role of frontoparietal loops in executive-motor integration during child development.

VIII. Discussion and Conclusion

This study demonstrates *Enriched Topological Features* (ETF) as a statistically validated and physiologically interpretable method for decoding cognitive brain states from

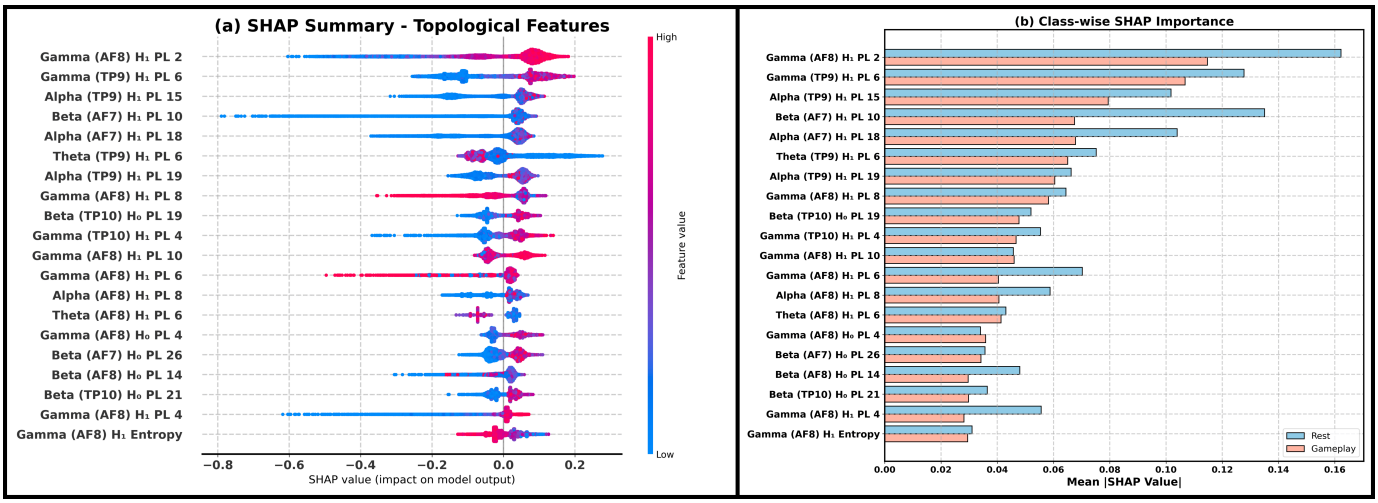

Fig. 4: Model interpretability via SHAP-based analysis of topological EEG features. (a) SHAP summary plot showing the top 20 features ranked by impact on classifier output. Each dot represents a SHAP value for an instance, colored by the corresponding feature value. (b) Class-wise SHAP importance plot, displaying the mean absolute SHAP values for rest and gameplay conditions separately. Higher bars indicate greater relevance of a feature to the respective class prediction. Feature labels follow the format: *Band (Channel) Homology LandscapeType Index*, where *Band* is the EEG frequency band (e.g., Gamma), *Channel* is the electrode (e.g., AF8), *Homology* refers to the topological dimension ($\mathbb{H}_0$ or $\mathbb{H}_1$), *LandscapeType* is either PL (Persistence Landscape) or Entropy, and *Index* denotes the specific component (e.g., PL 2).

low-density pediatric EEG acquired in naturalistic settings. By integrating persistent homology, time-aggregated entropy, and phase-space embeddings, ETF achieved 94.96% test accuracy with a 97.2% F1 score in distinguishing gameplay from rest thereby surpassing prior benchmarks like NETDA. These results confirm that topological data analysis provides a principled approach for extracting neural features stable under motion and recording variability even under environmental noise, participant movement and low spatial resolution.

Critically, ETF advances the field through both performance gains and neurophysiological interpretability. SHAP-based attribution revealed distinct topological signatures: gameplay engagement manifested as elevated gamma-band persistence landscapes at frontal sites, particularly AF8 $\mathbb{H}_1$ PL 2, reflecting executive network recruitment during goal-directed behavior [39]. Conversely, resting states showed high alpha-band entropy at temporal electrodes like TP9, indicating metastable disengagement consistent with default-mode network dynamics [40]. We also observed lateralized asymmetries in beta and gamma activity, with left frontal features showing stronger task associations, aligning with known developmental trajectories where parietal-cerebellar pathways support visuomotor coordination [41]. Notably, children exhibited topologically unstable gamma landscapes with shorter feature lifespans compared to adults, suggesting immature top-down control [42]. ETF captured this developmental distinctiveness by identifying compensatory dynamics like transient gamma–beta coupling.

Methodologically, ETF advances beyond previous frameworks through three key innovations: integration of features from multiple homology dimensions with entropy measures, temporal aggregation of persistence landscapes via sliding windows, and rigorous subject-level validation with class balancing techniques. Statistical validation confirmed ETF's superiority over benchmarks with p-values below 0.01. The framework maintains computational efficiency, processing each 4.5-second EEG epoch in approximately 644 milliseconds, enabling deployment on limited hardware.

The age-related decline in gamma-band $\mathbb{H}_1$ loop persistence aligns with established principles of developmental neurobiology. As shown in Figure 5, a statistically significant negative correlation was observed between age and the $\mathbb{H}_1$ persistence landscape lifespan (PL 2) at AF8 as the top SHAP-ranked gamma-band feature across the 6–16 year-old cohort ($r = -0.23$, $p = 0.0176$, 95% CI: $[-0.38, -0.07]$). Older children exhibited less persistent topological features, indicating briefer or less pronounced oscillatory loops in frontal gamma activity during gameplay. This trend is consistent with synaptic pruning and network refinement during development [38], [43], whereby the brain transitions from a state of exuberant local connectivity and high synaptic density to one of selective, efficient circuitry. These changes reduce the lifespan of gamma-band loops by minimizing the need for sustained high-frequency reverberations.

Longitudinal EEG studies show that gamma power peaks around age 4 and gradually decreases through adolescence, mirroring the decline in synaptic density [43]. Concurrently, pediatric fMRI studies reveal a transition from locally redundant networks to more distributed, integrated topologies [44]. As cortico-cortical pathways become more

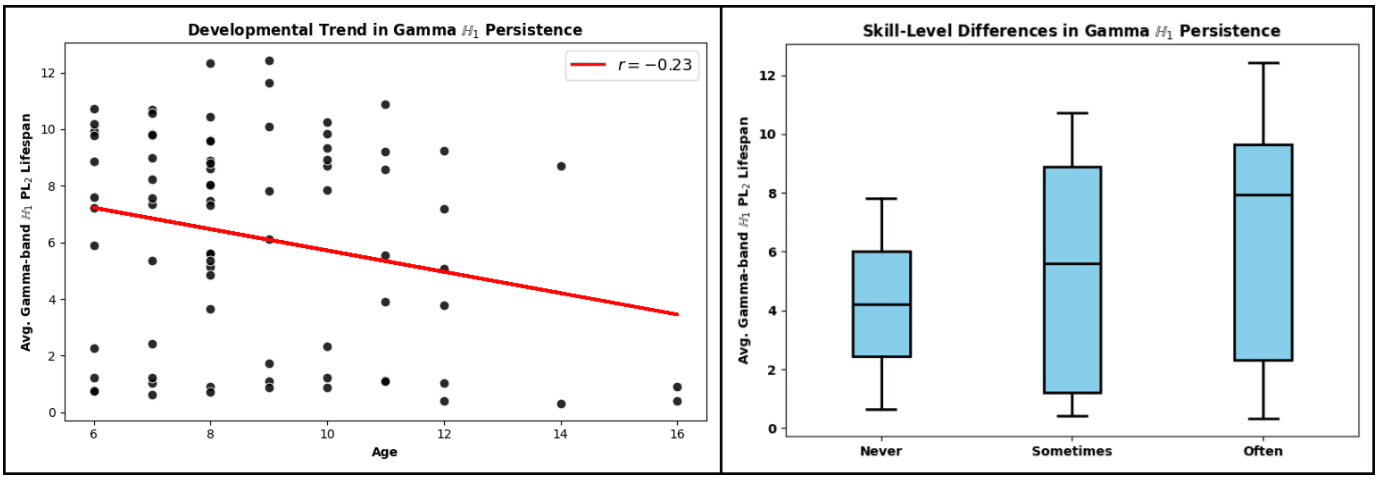

Fig. 5: **Topological dynamics of frontal gamma activity across age and gameplay experience. Left:** The average lifespan of the $\mathbb{H}_1$ persistence landscape layer 2 (PL_2) at AF8 during gameplay exhibited a significant negative correlation with age ($r = -0.23$, $p = 0.0176$), suggesting a developmental decrease in gamma-band topological stability. This trend may reflect maturational refinement of executive control networks during middle childhood and adolescence. **Right:** Group-level comparison across Minecraft gameplay frequency showed no significant differences (ANOVA: $F = 0.66$, $p = 0.52$), indicating that topological features were more strongly influenced by age than by gaming experience.

efficient, fewer and shorter-lived gamma oscillatory loops suffice to support executive function, leading to reduced $\mathbb{H}_1$ persistence in phase-space embeddings. In contrast, no significant differences in loop persistence were observed across Minecraft gameplay frequency groups (ANOVA: $F = 0.66$, $p = 0.52$), suggesting that biological maturation rather than gameplay exposure primarily shapes gamma-band topological structure. These findings support the interpretation of persistent gamma topology as a scalable, correlate of network maturation of network development.

This study has several limitations. The use of a four-channel EEG system restricts spatial resolution, limiting access to deeper or distributed cortical sources. Additionally, the binary classification framework does not capture finer-grained cognitive states such as flow, frustration, or disengagement during gameplay. Future extensions of the ETF framework will address these issues through multi-dimensional state decoding (e.g., via ordinal regression) and source localization techniques to enhance spatial interpretability.

While gamma-band persistence features at frontal sites (AF8) emerged as salient neural markers of gameplay engagement, interpreting high-frequency EEG activity in mobile pediatric contexts warrants caution [45]. To address concerns regarding potential artifact contamination, correlations between EEG amplitude and head motion energy derived from the Muse accelerometer were systematically analyzed across all 79 participants. The results revealed negligible associations (mean $r = 0.002$, median $r = 0.001$), with all $|r|$ values below 0.05 and none exceeding this threshold. These findings suggest that gross head motion did not systematically influence EEG signals, and by extension, the gamma-band features contributing to classification. Nonetheless, high-frequency EEG components particularly in the gamma band remain susceptible to myogenic artifacts originating from subtle facial muscle activity. Although the topological framework employed may offer intrinsic resilience to noise, future studies incorporating synchronized EMG monitoring will be necessary to definitively disentangle neurogenic and myogenic sources in naturalistic pediatric neuroimaging.

In conclusion, ETF improves both accuracy and interpretability over existing methods for pediatric EEG classification in naturalistic settings. Its integration of topological descriptors, efficient computation, and physiologically grounded features makes it well-suited for applied use in neurogaming, adaptive learning, and mobile cognitive monitoring. The framework's tolerance to noise and low-latency processing supports its deployment in real-world pediatric neuroengineering contexts.

Ethical Approval

This work uses the public dataset described in [46] available on IEEE DataPort under doi:10.21227/H23W88.

References

[1] D. E. Anderson and S. Perone, "Social eeg: A novel neurodevelopmental approach to studying brain-behavior links and brain-to-brain synchrony during naturalistic toddler-parent interactions," *Developmental Psychobiology*, vol. 60, no. 3, pp. 409–423, 2018.

[2] L. Schilbach, B. Timmermans, V. Reddy, A. Costall, G. Bente, T. Schlicht, and K. Vogeley, "Toward a second-person neuroscience," *Behavioral and Brain Sciences*, vol. 36, no. 4, pp. 393–414, 2013.

[3] C. Yu and L. B. Smith, "Infant sustained attention but not joint attention to objects predicts vocabulary at 2 years," *Developmental Science*, vol. 19, no. 1, pp. 126–138, 2016.

[4] A. Giannadou, M. Jones, M. Freeth, A. C. Samson, and E. Milne, "Investigating neural dynamics in autism spectrum conditions outside of the laboratory using mobile electroencephalography," *Psychophysiology*, vol. 59, no. 4, p. e13995, 2022.

[5] E. S. Norton, B. L. Manning, E. M. Harriott, J. I. Nikolaeva, O. S. Nyabingi, K. M. Fredian, J. M. Page, S. McWeeny, S. Krogh-Jespersen, L. A. MacNeill *et al.*, "Social eeg: A novel neurodevelopmental approach to studying brain-behavior links and brain-to-brain synchrony during naturalistic toddler–parent interactions," *Developmental Psychobiology*, vol. 64, no. 3, p. e22240, 2022.

[6] S. Georgieva, S. Lester, V. Noreika, M. N. Yilmaz, S. Wass, and V. Leong, "Toward the understanding of topographical and spectral signatures of infant movement artifacts in naturalistic eeg," *Frontiers in Neuroscience*, vol. 14, p. 352, 2020.

[7] S. Makeig, K. Gramann, T.-P. Jung, T. J. Sejnowski, and H. Poizner, "Linking brain, mind and behavior," *Proceedings of the IEEE*, vol. 100, no. Special Centennial Issue, pp. 528–541, 2009.

[8] K. Gramann, J. T. Gwin, N. Bigdely-Shamlo, D. P. Ferris, and S. Makeig, "Cognition in action: Imaging brain/body dynamics in mobile humans," *Reviews in the Neurosciences*, vol. 25, no. 3, pp. 365–380, 2014.

[9] S. Ladouce, D. I. Donaldson, P. A. Dudchenko, and M. Ietswaart, "Understanding minds in real-world environments: Toward a mobile cognition approach," *Frontiers in Human Neuroscience*, vol. 10, p. 694, 2017.

[10] X. Xu, N. Drougard, and R. N. Roy, "Topological data analysis as a new tool for eeg processing," *Frontiers in Neuroscience*, vol. 15, p. 761703, 2021.

[11] A. S. Ravindran, A. Mobiny, J. G. Cruz-Garza, A. Paek, A. Kopteva, and J. L. C. Vidal, "Assaying neural activity of children during video game play in public spaces: A deep learning approach," *Journal of Neural Engineering*, vol. 16, no. 3, p. 036028, 2019.

[12] M. Saggar, O. Sporns, J. Gonzalez-Castillo, P. A. Bandettini, G. Carlsson, G. Glover, and A. L. Reiss, "Towards a new approach to reveal dynamical organization of the brain using topological data analysis," *Nature Communications*, vol. 9, no. 1, p. 1399, 2018.

[13] N. Aithal, D. Bhattacharya, N. Sinha, and T. G. Issac, "Leveraging persistent homology for differential diagnosis of mild cognitive impairment," in *International Conference on Pattern Recognition*. Springer, 2025, pp. 17–32.

[14] K. Gaurav, J. Landge, and T. K. R. Bollu, "Characterizing neural activity during video game engagement using eeg sensor based topological dynamics analysis," *IEEE Sensors Letters*, 2024.

[15] A. Zomorodian and G. Carlsson, "Computing persistent homology," in *Proceedings of the Twentieth Annual Symposium on Computational Geometry*, 2004, pp. 347–356.

[16] Edelsbrunner, Letscher, and Zomorodian, "Topological persistence and simplification," *Discrete & Computational Geometry*, vol. 28, pp. 511–533, 2002.

[17] P. Bubenik *et al.*, "Statistical topological data analysis using persistence landscapes," *Journal of Machine Learning Research*, vol. 16, no. 1, pp. 77–102, 2015.

[18] N. Atienza, R. Gonzalez-Diaz, and M. Rucco, "Persistent entropy for separating topological features from noise in vietoris-rips complexes," *Journal of Intelligent Information Systems*, vol. 52, pp. 637–655, 2019.

[19] A. S. Ravindran, J. Cruz-Garza, A. Kopteva, A. Paek, A. Mobiny, Z. Hernandez, and J. Contreras-Vidal, "Multi-modal mobile brain-body imaging (mobi) dataset for assaying neural and head movement responses associated with creative video game play in children," *IEEE Dataport*, 2017, available from: https://doi.org/10.21227/H23W88.

[20] A. Widmann, E. Schröger, and B. Maess, "Digital filter design for electrophysiological data—a practical approach," *Journal of Neuroscience Methods*, vol. 250, pp. 34–46, 2015.

[21] P. Welch, "The use of fast fourier transform for the estimation of power spectra: A method based on time averaging over short, modified periodograms," *IEEE Transactions on Audio and Electroacoustics*, vol. 15, no. 2, pp. 70–73, 2003.

[22] F. Takens, "Detecting strange attractors in turbulence," in *Dynamical Systems and Turbulence, Warwick 1980: Proceedings of a Symposium Held at the University of Warwick 1979/80*. Springer, 2006, pp. 366–381.

[23] A. M. Fraser and H. L. Swinney, "Independent coordinates for strange attractors from mutual information," *Physical Review A*, vol. 33, no. 2, p. 1134, 1986.

[24] M. B. Kennel, R. Brown, and H. D. I. Abarbanel, "Determining embedding dimension for phase-space reconstruction using a geometrical construction," *Physical Review A*, vol. 45, no. 6, p. 3403, 1992.

[25] N. V. Chawla, K. W. Bowyer, L. O. Hall, and W. P. Kegelmeyer, "Smote: Synthetic minority over-sampling technique," *Journal of Artificial Intelligence Research*, vol. 16, pp. 321–357, 2002.

[26] H. He and E. A. Garcia, "Learning from imbalanced data," *IEEE Transactions on Knowledge and Data Engineering*, vol. 21, no. 9, pp. 1263–1284, 2009.

[27] A. Shen, J. Sun, X. Chen, and X. Gao, "A data-centric and interpretable eeg framework for depression severity grading using shap-based insights," *Journal of NeuroEngineering and Rehabilitation*, vol. 22, no. 1, pp. 1–16, 2025.

[28] F. Lotte, L. Bougrain, A. Cichocki, M. Clerc, M. Congedo, A. Rakotomamonjy, and F. Yger, "A review of classification algorithms for eeg-based brain–computer interfaces: A 10 year update," *Journal of Neural Engineering*, vol. 15, no. 3, p. 031005, 2018.

[29] L. Breiman, "Random forests," *Machine Learning*, vol. 45, pp. 5–32, 2001.

[30] S. Varma and R. Simon, "Bias in error estimation when using cross-validation for model selection," *BMC Bioinformatics*, vol. 7, pp. 1–8, 2006.

[31] M. Sokolova and G. Lapalme, "A systematic analysis of performance measures for classification tasks," *Information Processing & Management*, vol. 45, no. 4, pp. 427–437, 2009.

[32] S. M. Lundberg and S.-I. Lee, "A unified approach to interpreting model predictions," *Advances in Neural Information Processing Systems*, vol. 30, 2017.

[33] M. W. Howard, D. S. Rizzuto, J. B. Caplan, J. R. Madsen, J. Lisman, R. Aschenbrenner-Scheibe, A. Schulze-Bonhage, and M. J. Kahana, "Gamma oscillations correlate with working memory load in humans," *Cerebral Cortex*, vol. 13, no. 12, pp. 1369–1374, 2003.

[34] F. Aoki, E. E. Fetz, L. Shupe, E. Lettich, and G. A. Ojemann, "Increased gamma-range activity in human sensorimotor cortex during performance of visuomotor tasks," *Clinical Neurophysiology*, vol. 110, no. 3, pp. 524–537, 1999.

[35] L. Pei, G. Northoff, and G. Ouyang, "Comparative analysis of multifaceted neural effects associated with varying endogenous cognitive load," *Communications Biology*, vol. 6, no. 1, p. 795, 2023.

[36] P.-M. Matta, R. Baurès, J. Duclay, and A. Alamia, "Modulation of beta oscillatory dynamics in motor and frontal areas during physical fatigue," *Communications Biology*, vol. 8, no. 1, p. 687, 2025.

[37] W. Klimesch, P. Sauseng, and S. Hanslmayr, "Eeg alpha oscillations: The inhibition–timing hypothesis," *Brain Research Reviews*, vol. 53, no. 1, pp. 63–88, 2007.

[38] P. J. Uhlhaas, F. Roux, E. Rodriguez, A. Rotarska-Jagiela, and W. Singer, "The development of neural synchrony reflects late maturation and restructuring of functional networks in humans," *Proceedings of the National Academy of Sciences*, vol. 106, no. 24, pp. 9866–9871, 2009.

[39] M. Assem, M. G. Hart, P. Coelho, R. Romero-Garcia, A. McDonald, E. Woodberry, R. C. Morris, S. J. Price, J. Suckling, T. Santarius *et al.*, "High gamma activity distinguishes frontal cognitive control regions from adjacent cortical networks," *Cortex*, vol. 159, pp. 286–298, 2023.

[40] Y.-W. Kim, S. Kim, M. J. Jin, C.-H. Im, and S.-H. Lee, "The importance of low-frequency alpha (8–10 hz) waves and default mode network in behavioral inhibition," *Clinical Psychopharmacology and Neuroscience*, vol. 22, no. 1, p. 53, 2023.

[41] E. Ünsal, R. Duygun, İ. Yemeniciler, E. Bingöl, Ö. Ceran, and B. Güntekin, "From infancy to childhood: A comprehensive review of event-and task-related brain oscillations," *Brain Sciences*, vol. 14, no. 8, p. 837, 2024.

[42] A. Pines, A. S. Keller, B. Larsen, M. Bertolero, A. Ashourvan, D. S. Bassett, M. Cieslak, S. Covitz, Y. Fan, E. Feczko *et al.*, "Development of top-down cortical propagations in youth," *Neuron*, vol. 111, no. 8, pp. 1316–1330, 2023.

[43] S. D. McKeon, F. Calabro, R. V. Thorpe, A. de la Fuente, W. Foran, A. C. Parr, S. R. Jones, and B. Luna, "Age-related differences in transient gamma band activity during working memory maintenance through adolescence," *NeuroImage*, vol. 274, p. 120112, 2023.

[44] D. A. Fair, A. L. Cohen, J. D. Power, N. U. F. Dosenbach, J. A. Church, F. M. Miezin, B. L. Schlaggar, and S. E. Petersen, "Functional brain networks develop from a "local to distributed" organization," *PLoS Computational Biology*, vol. 5, no. 5, p. e1000381, 2009.

[45] A. J. Shackman, B. W. McMenamin, H. A. Slagter, J. S. Maxwell, L. L. Greischar, and R. J. Davidson, "Electromyogenic artifacts and electroencephalographic inferences," *Brain Topography*, vol. 22, pp. 7–12, 2009.

[46] "Multi-modal mobile brain-body imaging (mobi) dataset for assaying neural and head movement responses associated with

creative video game play in children," 2017. [Online]. Available: https://dx.doi.org/10.21227/H23W88